THE ASTROPHYSICAL JOURNAL, 466:957–963, 1996 August 1

POSSIBLE INFALL IN THE GAS DISK AROUND L1551-IRS 5[1]

NAGAYOSHI OHASHI,[2] MASAHIKO HAYASHI,[3] PAUL T. P. HO,[2] MUNETAKE MOMOSE,[4] AND NAOMI HIRANO[5]

Received 1995 November 27; accepted 1996 February 12

ABSTRACT

We report observations of $^{13}CO(J = 1–0)$ emission from L1551-IRS5 carried out with the Nobeyama Millimeter Array. We detected a strong and compact condensation associated with L1551-IRS5, and weaker extended components with "U"-like features with a spatial resolution of 5″.1 × 3″.9 (P.A. = 159°). The U-like features delineate the edges of the molecular outflow as well as the 2.2 μm infrared reflection nebula. This suggests that the extended component may be a dense shell swept up by the molecular outflow. The compact component was marginally resolved with the present angular resolution. The estimated deconvolved size is $\sim 1200 \times 670$ AU with a position angle perpendicular to the optical jet. This elongated structure is very similar to the compact gaseous disk observed in $C^{18}O$ ($J = 1–0$). The ^{13}CO elongated structure may be more extended than the actually measured size, suggesting that the compact ^{13}CO gas is most probably the inner part of the gaseous disk around L1551-IRS5. The ^{13}CO disk has a velocity gradient along its minor axis, which can be explained in terms of infalling motion in the plane of the disk with a central mass of 0.5 $M_\odot$. We estimate the mass accretion rate at 600 AU in radius to be $1.3–2.6 \times 10^{-5}$ $M_\odot$ yr^{-1}. The derived accretion rate might be larger than the accretion rate onto the star estimated from the bolometric luminosity of L1551-IRS5 on the assumption of steady accretion, which suggests that the accretion around L1551-IRS5 may also be nonsteady as was the case for HL Tau.

Subject headings: accretion, accretion disks — circumstellar matter — ISM: molecules — ISM: structure — stars: formation — stars: individual (L1551-IRS5) — stars: pre–main sequence

1. INTRODUCTION

Dynamical infall is essential in star formation because dense molecular cloud cores dynamically collapse to form stars due to the isothermal nature of interstellar gas. Deeply embedded sources observed with *Infrared Astronomical Satellite* (*IRAS*) in nearby star forming regions are the best candidates of low-mass accreting protostars with dynamically infalling envelopes (Beichman et al. 1986). It is important to obtain direct evidence of dynamical infall toward embedded protostar candidates because this is a way to identify a "real" protostar without any ambiguity. There is indirect evidence for infall around these embedded sources, e.g., their spectral energy distributions (Adams, Lada, & Shu 1987; Kenyon, Calvet, & Hartmann 1993), their asymmetric line profiles (Zhou 1992; Zhou et al. 1993; Myers et al. 1995), and their circumstellar mass distribution in comparison with revealed T Tauri stars (Ohashi et al. 1991, 1996). Since the infall velocity scales as the inverse square root of the distance from a central protostar, high spatial and spectral resolutions are necessary to detect infalling motion. Recent high-resolution observations have revealed a dynamically infalling disk toward the young T Tauri star HL Tau (Hayashi, Ohashi, & Miyama 1993, hereafter HOM), suggesting that HL Tau is actually an accreting protostar with a visible reflection nebula.

In this paper, we report ^{13}CO ($J = 1–0$) observations of L1551-IRS5, a prototypical embedded protostar candidate with a strong molecular outflow (Snell, Loren, & Plambeck 1980; Moriarty-Schieven & Snell 1988), an optical jet (Mundt & Fried 1983; Stocke et al. 1988), and a circumstellar disk. Pioneering observations of the gaseous disk around L1551-IRS5 have been made by Kaifu et al. (1984), who revealed a disklike structure of 0.05 pc in radius. Sargent et al. (1988, hereafter SBKM), by observing $C^{18}O(J = 1–0)$ with the Owens Valley Radio Observatory (OVRO) interferometer, have shown smaller scale structures of the gaseous disk with a radius of ~ 700 AU. An even more compact inner disk was suggested by interferometric measurements of the dust emission at 3 mm wavelength with the OVRO (Keene & Masson 1990) and at submillimeter wavelength with the JCMT-CSO interferometer (Lay et al. 1994). A size scale of ~ 80 AU for the inner disk is suggested from visibility plots. This inner disk appears to be ionized on its inner portion as suggested by VLA observations at 2 cm with a resolution of $\sim 0''.15$ (Rodríguez et al. 1986).

We report here new observations of L1551-IRS5 with the Nobeyama Millimeter Array in the $^{13}CO(J = 1–0)$ line in order to study the detailed velocity field of the gas disk. The obtained data show a velocity structure consistent with infalling motion in the plane of the disk. We will discuss the nature of this contracting disk around L1551-IRS5.

2. OBSERVATIONS

Observations of $^{13}CO(J = 1–0)$ were made using the Nobeyama Millimeter Array (NMA) in 1993 December with the D-configuration and in 1995 February with the

[1] Based on observations made at the Nobeyama Radio Observatory (NRO). NRO is a branch of the National Astronomical Observatory, an interuniversity research institute operated by the Ministry of Education, Science, and Culture of Japan.

[2] Harvard-Smithsonian Center for Astrophysics, MS78, 60 Garden Street, Cambridge, MA 02138; nohashi, pho@cfa.harvard.edu.

[3] SUBARU Project Office, National Astronomical Observatory, Mitaka, Tokyo 181, Japan; masa@optik.mtk.nao.ac.jp.

[4] Department of Astronomical Science, The Graduate University for Advanced Studies, Nobeyama Radio Observatory, Minamimaki, Minamisaku, Nagano 384-13, Japan; momose@nro.nao.ac.jp.

[5] Laboratory of Astronomy and Geophysics, Hitosubashi University, Kunitachi, Tokyo 186, Japan; hirano@higashi.hit-u.ac.jp.

C-configuration. We used 4 K cooled SIS tunerless receivers (Sunada, Kawabe, & Inatani 1993), the system noise temperatures of which were typically $\sim$400 K (double-side band). Spectral information were provided by the FX digital correlator (Chikada et al. 1987) with 160 MHz frequency coverage and 1024 spectral channels, corresponding to $\sim$0.425 km s^{-1} velocity resolution at the ^{13}CO line. Two tracks of data were taken with four 10 m dishes in the D-configuration, and one track of data with six 10 m dishes in the C-configuration. A total of 21 independent baselines were obtained. The shortest projected baseline was $\sim$13 m, which made our observations insensitive to structures extended more than $\sim$43″ (6000 AU). Antenna phase and gain calibrations were made by observing 0528+134 every 30 minutes. The complex pass band of the FX correlator was determined by observing 3C454.3 for 40 minutes. After subtracting continuum emission from the calibrated *u-v* data and combining them, we CLEANed each ^{13}CO channel map by using the Astronomical Image Processing System (AIPS) package. Natural weight was applied to the *u-v* data, and the resultant beam size was 5″.1 × 3″.9 (P.A. = 159°; FWHM) with sidelobe levels less than 20% of the main beam.

We also made a 2.7 mm continuum map by averaging the line-free channels. Unresolved 2.7 mm continuum emission with a total flux density of $\sim$160 mJy was detected, with the same angular resolution as the ^{13}CO map. This is consistent with previous interferometric observations (Keene & Masson 1990; Ohashi et al. 1991), meaning that the observed flux density was well calibrated. The peak position of the 2.7 mm continuum is coincident with the 2 cm radio continuum position (Rodríguez et al. 1986). We will adopt our 2.7 mm continuum peak as the position of L1551-IRS5 in this paper.

3. RESULTS

^{13}CO (J = 1–0) emission was detected in the LSR velocity range of 4.3–8.5 km s^{-1} with a typical sensitivity of $\sim$150 mJy beam^{-1} (1 σ) for each channel map. In Figure 1 (Plate 19), we show the ^{13}CO map integrated over the detected velocity range superimposed on an image of the 2.2 μm infrared reflection nebula (Hodapp 1994). The integrated intensity map indicates that the detected emission consists of two parts: a compact component with a peak coincident with the position of L1551-IRS5, and a diffuse extended component elongated from north to south across L1551-IRS5. We discuss these two components in more detail below.

3.1. *Compact Component: Gaseous Disk*

The compact component, which has a strong peak exactly coincident with the stellar position and a weaker feature extended around it at the 4 σ contour level, was marginally resolved with the present angular resolution. The deconvolved size is 8″.3 × 4″.8, corresponding to 1200 × 670 AU at the distance of L1551-IRS5 (140 pc; Elias 1978). Its position angle of $\sim$155° is almost perpendicular to the optical jet observed in [S II] (Stocke et al. 1988) and the radio jet observed at 2 cm (Rodríguez et al. 1986). This elongated structure, perpendicular to the jet, suggests that the compact ^{13}CO condensation is most probably a gaseous disk around L1551-IRS5. The detected disklike structure is basically consistent with that of the C^{18}O compact disk observed by SBKM. However, the position angle of the C^{18}O disk is $\sim$135° at 3″.5 resolution and $\sim$160° at 6″.5 resolution. This difference in position angle may be a resolution effect where small scale structures may show different position angles depending on whether they are resolved. Note also that recent JCMT-CSO observations of L1551-IRS5 have shown that the compact dust disk, which traces the most inner part of the gaseous disk, has a position angle of 153°–180° (Lay et al. 1994).

Our derived size indicates that the disk is nearly edge-on rather than face-on. We estimate that the disk is inclined $\sim$55° with respect to the plane of the sky (90° for edge-on). This inclination angle is a lower limit, because the disk is not clearly resolved along its minor axis, and is consistent with the value derived from the JCMT-CSO observations (Lay et al. 1994). It is important to note that the infrared reflection nebula and optical jet extend to the southwest of the disk as was shown in Figure 1, suggesting that the disk is inclined with its northeast part located on the near side and its southwest part on the far side.

Figure 2 (Plate 20), showing the mean-velocity map of ^{13}CO, demonstrates that the disk has a velocity gradient along its minor axis: the mean-velocity of the ^{13}CO emission increases from 5.0–7.5 km s^{-1} along the minor axis of the disk from southwest to northeast, parallel to the axis of the optical jet. Because the systemic velocity of the molecular cloud associated with L1551-IRS5 is $\sim$6.2 km s^{-1}, the northeastern part (i.e., near side) of the disk is redshifted and the southwestern part (i.e., far side) is blueshifted.

Note that the emissions with highly blueshifted and redshifted velocities are not apparent in Figure 2 both because of their weakness and the process of computing the mean velocity. To see the structure at higher velocities, we must examine the individual channels. In Figure 3, we see that at the most blueshifted velocity 4.5 km s^{-1}, weak emission is detected at the position of the central star. At 4.92 km s^{-1}, the emission is almost unresolved, with the peak located at $\sim$2″ south of the central source. The strongest emission is detected at 5.35 km s^{-1}, with a core component which is elongated from northwest to southeast across L1551-IRS5 and centers at $\sim$2″ south of the central source. There is a weaker extension to the southwest of the core with faint extended structures to the south. At 5.77, 6.2, and 6.62 km s^{-1}, which are close to the systemic velocity ($\sim$6.2 km s^{-1}), the central core component appears much fainter. Weak emission appears centered at $\sim$2″–5″ northwest of the star at 5.77 and 6.2 km s^{-1}, and at $\sim$2″ southwest of the star at 6.62 km s^{-1}. For these three velocity channels, our observations detected at most 10% of the total flux observed with the Nobeyama 45 m telescope, indicating that most of the emission was resolved out because of the lack of short spacing data. Thus, details of the observed structures in these three velocity channels may not be reliable. The central component reappears at 7.04 km s^{-1}. The emission is elongated to the northeast from the central position at higher contour levels, and is slightly extended to the southeast at lower levels. There are faint emissions both to the north and south. The emission at 7.47 km s^{-1} is centered at $\sim$2″ northeast of the star, and is almost unresolved with the present resolution. Fainter emissions are again present to the north and southeast. At 7.89 and 8.32 km s^{-1}, weak emission is detected at the central source position. The above inspection of the channel maps shows the trend where the southwestern part of the disk is blueshifted and the northeastern part is redshifted, as also shown in Figure

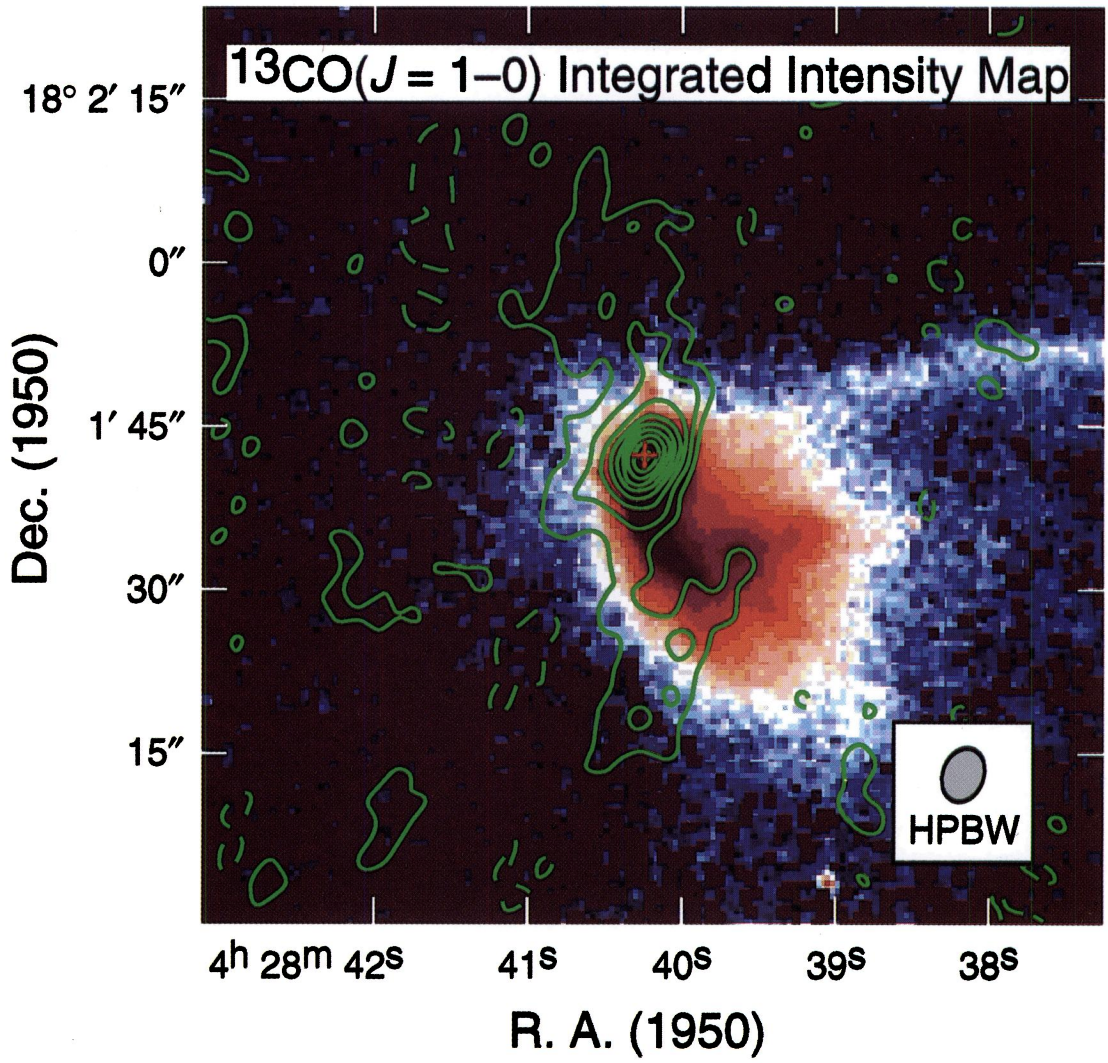

FIG. 1.—^{13}CO (J = 1–0) map of L1551-IRS5 integrated in the velocity range of 4.3–8.5 km s^{-1}. Contours are drawn every 2 σ from the 2 σ level for the positive contours (*green lines*), and from the -2 σ level for the negative contours (*green dashed lines*). The 1 σ level corresponds to 46.2 mJy beam^{-1}. For comparison, the 2.2 μm infrared reflection nebula observed by Hodapp (1994) were superimposed in pseudocolor. The red cross marks the position of L1551-IRS5 as defined by the 110 GHz continuum position in this work.

OHASHI et al. (see 466, 958)

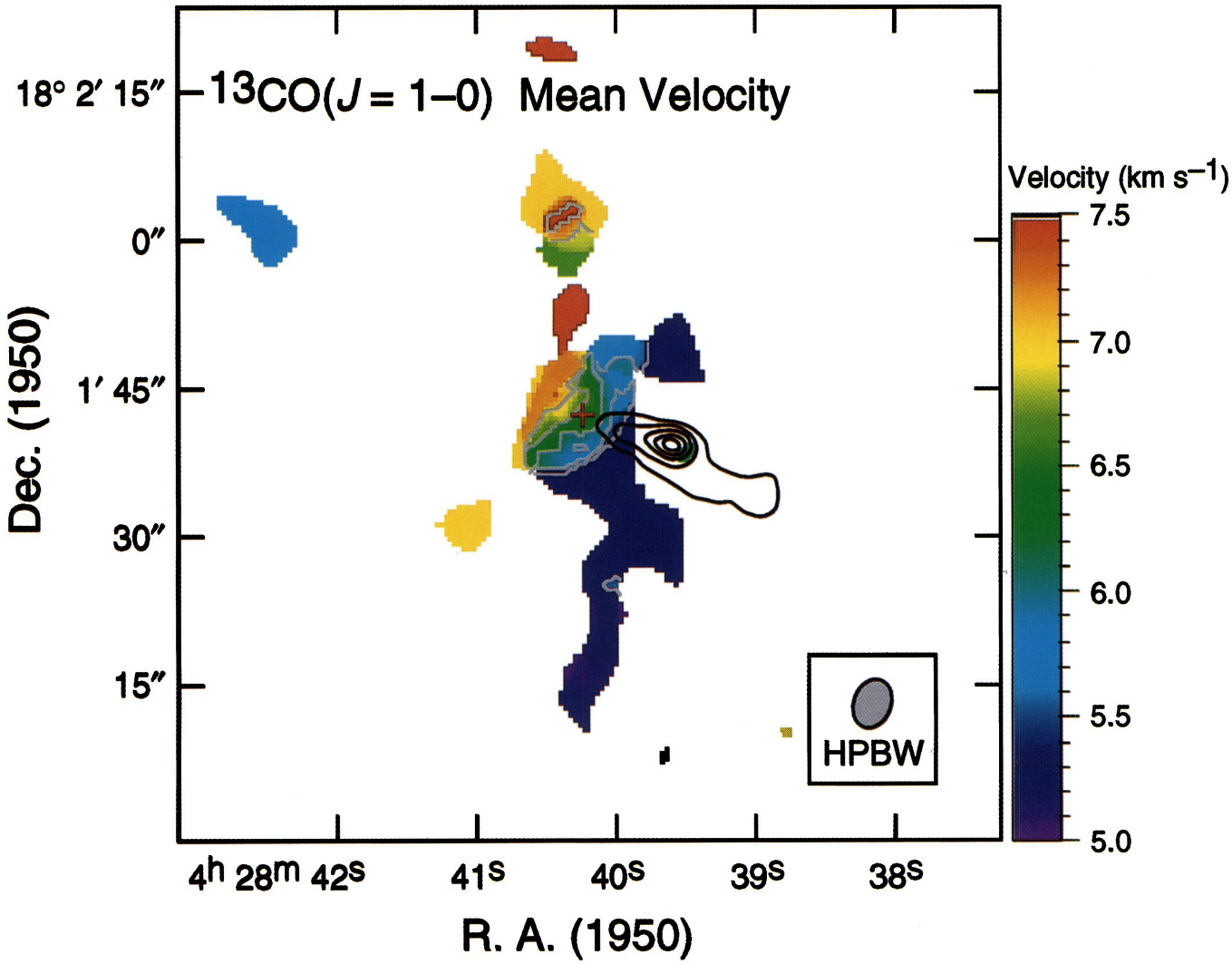

FIG. 2.—Mean velocity map of ^{13}CO (J = 1–0) emission toward L1551-IRS5 is presented in pseudocolor. Contours are drawn every 0.4 km s^{-1} from 5.4 km s^{-1}. Systemic LSR velocity of the cloud associated with L1551-IRS5 is ~6.2 km s^{-1}. For comparison, the optical jet in [S II] observed by Stocke et al. (1988) is superimposed in red contours with shade. The red cross marks the position of L1551-IRS5 as defined by the 110 GHz continuum position in this work.

OHASHI et al. (see 466, 958)

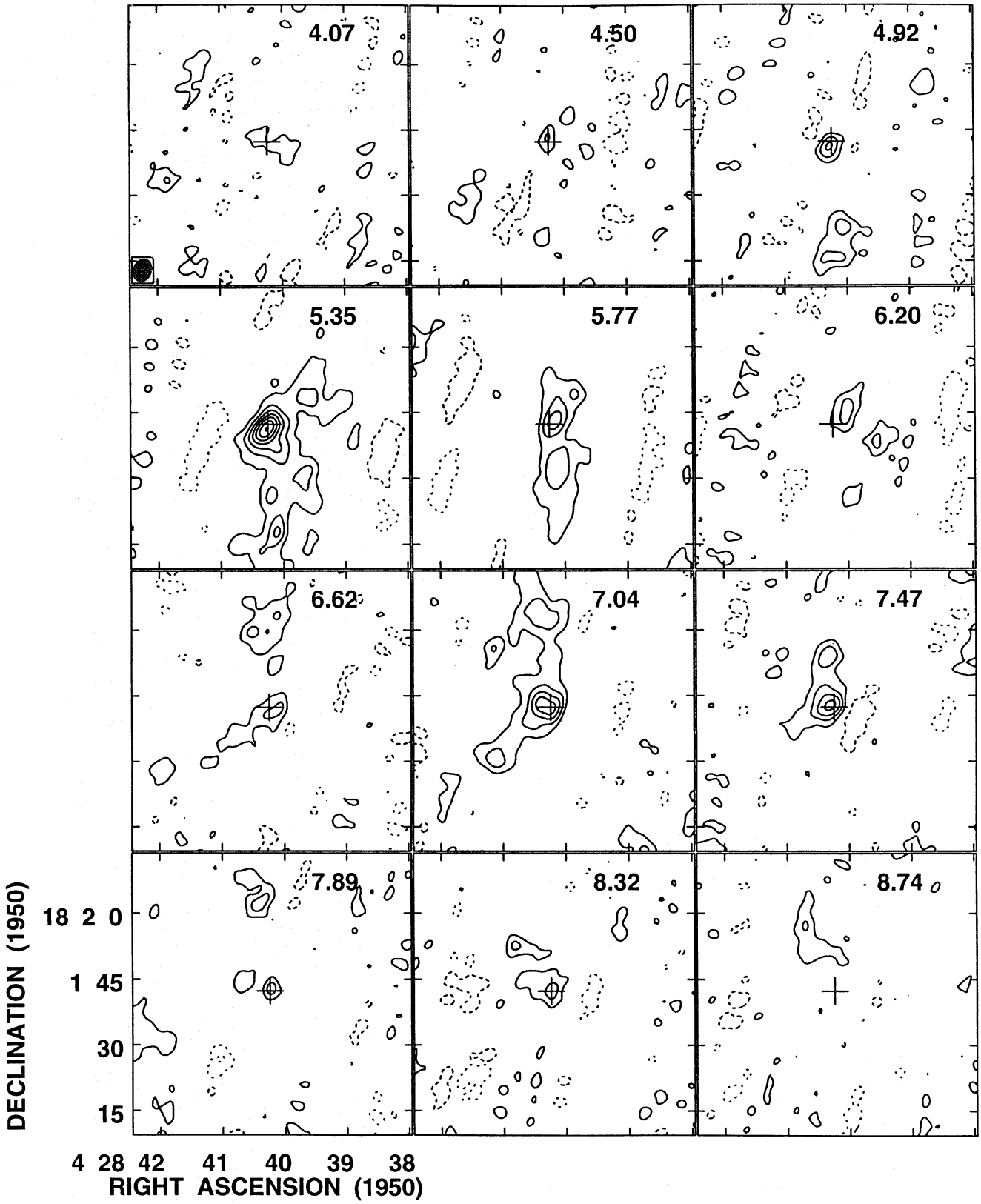

FIG. 3.—Channel velocity maps of ^{13}CO ($J = 1$–0). Corresponding LSR velocities are denoted in the top right corner in each panel. Contours are drawn in the same manner as in Fig. 1. The 1 σ level corresponds to 147 mJy beam^{-1} with the velocity resolution of 0.425 km s^{-1}. The cross in each panel marks the position of L1551-IRS5, and the hatched ellipse in the top left panel indicates the beam size in FWHM.

2. In addition, the channel maps tell us another crucial trend that higher blueshifted (4.50 and 4.92 km s^{-1}) and redshifted (7.89 and 8.32 km s^{-1}) velocity components are confined to the stellar position.

Such trends of the velocity structure of the disk are more clearly demonstrated in the position-velocity diagram along the minor axis of the disk as shown in Figure 4. At higher blueshifted ($\lesssim$5 km s^{-1}) and redshifted ($\gtrsim$8 km s^{-1}) veloci-

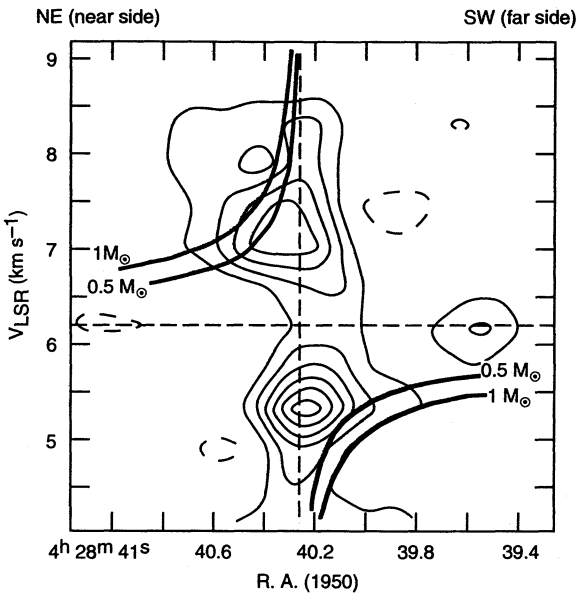

FIG. 4.—Position velocity diagram of ^{13}CO (J = 1–0) cutting along the minor axis of the disk (P.A. = 65°) through the position of L1551-IRS5. Contours are drawn in the same manner as in Fig. 1. The velocity resolution is 0.425 km s^{-1}, and the angular resolution is 4.″6 or 0.^{s}31 in the projected Right Ascension. Vertical and horizontal dashed lines indicate the position of L1551-IRS5 and the systemic LSR velocity of the disk, respectively. Two thick curves demonstrate radial velocity distributions of a dynamical infalling disk along its minor axis with a central star of 1 $M_\odot$ (*outer curve*) and 0.5 $M_\odot$ (*inner curve*), respectively, on the assumption of a disk inclination angle of 55°.

ties, the emission is confined to the vicinity of the central star, while the emission with lower redshifted and blueshifted velocities are extended to the northeast (i.e., near side) and the southwest (i.e., far side) parts of the disk, respectively. If the velocity field shown in Figure 4 traces radial motion in the plane of the disk, then the far side of the disk with blueshifted radial velocities is moving toward us, while the near side with redshifted velocities is moving away from us. This can be understood as contraction of the disk as was observed for the ^{13}CO disk around HL Tau (HOM). The trend that higher blueshifted and redshifted emissions are confined to the position of the central star is consistent with the infalling interpretation, because infalling matter is accelerated as it approaches the central star. In fact, the entire velocity structure shown in Figure 4 is consistent with a radial velocity field of infalling matter, which is inversely proportional to the square root of the radius (see § 4.1.). We will discuss the infalling motion of the disk in detail in § 4.

We must note, however, that the strong molecular outflow associated with L1551-IRS5 has the same velocity gradient as shown in Figure 4 in the sense that the blueshifted lobe is located to the southwest of the central object and the redshifted lobe is located to the northeast of it. This might mean that the velocity gradient shown in Figure 4 could be due to the outflow rather than the radial motion of the disk (Cabrit et al. 1996). However, the central core component shows the elongated structure which is very similar to the C^{18}O disk (SKBM) as was shown in Figure 1, suggesting that the ^{13}CO emission detected in the central component is almost certainly arising from the disk rather than from the outflow. Moreover, we note that the molecular outflow associated with L1551-IRS5 shows a quasi-linear increase in its velocity with distance from the driving source even on a small scale (~1′) (Moriarty-Schieven & Snell 1988; see also Bachiller, Tafalla, & Cernicharo 1994; Cabrit & Bertout 1990; Masson & Chernin 1992). This suggests that the ^{13}CO gas should look apparently accelerated as it moves further from the central star, if the ^{13}CO emission and the detected velocity gradient actually trace the outflowing motion. However, the velocity field in Figure 4 shows the opposite trend, favoring the infall scenario.

The disk does not show a clear velocity gradient along the major axis, as would be expected for rotation. The peak positions of the emission at 4.9 km s^{-1} is slightly shifted to ~2″ southeast of the star, while that at 7.9 km s^{-1} is slightly shifted to the north of it. If this shift in position is due to rotation, the rotational velocity could be ~1.3–1.7 km s^{-1} at 280 AU in radius, which is roughly consistent with rotation of a Keplerian disk with a 0.5 $M_\odot$ central star. However, this is highly uncertain because the emission close to the systemic velocity is drastically resolved out in the present observations.

3.2. *Extended Component: Swept-up Shell*

The faint extended component shown in Figure 1 is elongated from north to south across the central object for ~50″, corresponding to 6300 AU, which is comparable to the field of view of the NMA. This suggests that the flux density of the extended component has been attenuated both due to the primary beam response, and the lack of short spacings. Thus we must investigate the extended component while noting the limitation of our data.

Comparing the ^{13}CO integrated intensity map with the 2.2 μm infrared reflection nebula (Hodapp 1994), we find that the southern part of the extended component corresponds very well with the eastern side of the reflection nebula. Thus, the southern part of the extended component seems to reflect the light from the central object. Although the integrated intensity map shows only simple structures of the extended component, the velocity channel maps presented in Figure 3 demonstrate more complicated features in addition to the north-south structure in Figure 1. The extended component was prominently detected at blueshifted velocities of 5.35 and 5.77 km s^{-1} and redshifted ones of 7.04 and 7.47 km s^{-1} with additional detection at 4.92, 6.62, and 7.89 km s^{-1}. At the blueshifted velocities, particularly at 5.35 km s^{-1}, the extended component is elongated to the south of the central object with an additional feature extending to the northwest: the overall morphology is U-shaped. The redshifted extended emission at 7.04 km s^{-1}, on the other hand, is elongated to the north with an additional feature extending to the southeast, which also seems to form a more widely opened U-shape. Such a U-shape could be an artifact of resolving out extended structures. However, single-dish data of ^{13}CO (J = 1–0) from L1551-IRS5 (Moriarty-Schieven & Snell 1988; see also Uchida et al. 1987 for ^{12}CO observations) also show a similar U-shape, suggesting that the U-shaped feature is real. Both blueshifted and redshifted U structures roughly delineate the blue and red lobes of the outflow, respectively. Moreover, when we compare the blueshifted U feature with the 2.2 μm reflection nebula shown in Figure 1, it is found that the reflection nebula is just located in the hollow of the U feature. These properties suggest that the extended component may be part of a dense shell swept up by the outflow, as has been observed toward several young stellar objects (YSOs) (e.g., Kitamura et al. 1992; Yang, Ohashi, & Fukui 1995; Ohashi et al. 1996). To study the shell structure

around L1551-IRS5 in more detail, we will need to carry out interferometric observations over adjacent fields in order to make a proper mosaic.

4. DISCUSSION

4.1. *Infalling Motion in the Disk around L1551-IRS5*

As was shown in § 3, it is found that the disk around L1551-IRS5 has a velocity gradient along its minor axis, which is naturally explained in terms of an infalling motion of the disk. In this section, we will discuss this infalling motion in the disk in more detail.

If the velocity gradient shown in Figure 4 is consistent with the contraction of the disk, the velocity field should show accelerating motions inversely proportional to the square root of the radius, i.e., $V_r \propto r^{-0.5}$. We compared the position-velocity diagram with radial velocity distribution of a dynamically infalling disk ($V_r = \sqrt{2GM_*/r}$, where M_* is the mass of the central star) on the assumption that the disk is inclined by 55°. The velocity gradient can be explained in terms of the dynamically infalling motion gravitationally bound by a central star of $\sim 0.5\ M_\odot$. This is consistent with the stellar mass estimated from the bolometric luminosity of L1551-IRS5 (33 $L_\odot$; Keene & Masson 1990) assuming that the age of L1551-IRS5 is $\sim 10^5$ yr. Strictly speaking, the detected ^{13}CO emission is located much closer to the central star than the positions expected from the velocity distribution around a 0.5 $M_\odot$ star. However, we must note that we assumed that the inclination angle of the disk is 55°, which may be a lower limit to the actual inclination angle. When we use an inclination angle of 75° estimated from studies of the outflow (Snell & Schloerb 1985; Liseau & Sandell 1986), the expected radial velocity distribution of infalling matter with a central star of 0.5 $M_\odot$ more resembles the observed velocity structure.

We note that our observations do not show that the disk is spatially thin, even though we have assumed that in the above discussion for the sake of simplicity. Our observations cannot tightly constrain the details of the disk structure because of insufficient spatial resolution and missing extended components. Nevertheless, the size of the infalling gas is ~ 1200 AU, which is more than 10 times larger than the inner compact disk observed in continuum emission with interferometers (Keene & Masson 1990; Lay et al. 1994). Such an extended structure may be part of the envelope surrounding the L1551-IRS5 inner compact disk. In this sense, we should regard the infalling disk as an infalling flattened envelope, as was predicted by a fitting to the spectral energy distribution of L1551-IRS5 (Kenyon et al. 1993).

If the infalling disk is a flattened envelope with relatively edge-on configuration as was discussed above, other evidence for infall around L1551-IRS5 may be given by the observed line profiles of ^{13}CO. According to Zhou (1992), asymmetric line profiles with stronger blueshifted emission are expected when we observe infalling envelopes in relatively optically thick line emission in the presence of a temperature gradient in the infalling matter: for redshifted emission arising from the front side of the infalling envelope with respect to the central star, its optical depth approaches unity relatively far away from the star where the temperature of the envelope is relatively low, while for blueshifted emission coming from the back side of the envelope, the foreground side is transparent so that the optical depth becomes unity at a position relatively close to the star where the temperature is relatively high. In principle, a similar phenomenon may be expected to occur in a flattened envelope with relatively edge-on configuration even though its exact details are different from the spherical case discussed by Zhou (1992). The ^{13}CO emission averaged in the 5″ × 5″ area around L1551-IRS5 actually shows an asymmetric profile with stronger blueshifted emission as presented in Figure 5, strengthening the case for infall. Note that the central dip of the profile is not due to self-absorption as seen in the asymmetric profiles taken by single-dish observations (Zhou 1992; Zhou et al. 1993; Myers et al. 1995), but due to resolving out the extended structures at low infalling velocities. Nevertheless, the asymmetric features of the ^{13}CO profile suggest that the blueshifted emission is closer to the center of the infalling disk as compared with the redshifted emission. A positional difference between the blueshifted and redshifted emission can be actually found in Figure 4: blueshifted emission with ~ 5.5 km s^{-1} LSR velocity is much closer to the central star than the redshifted emission with ~ 7 km s^{-1}.

4.2. *Physical Properties of the Infalling Disk*

We estimate the size of the disk to be 1200 AU from the integrated intensity map. We note that ^{13}CO emission in the range of ~ 5.6–6.8 km s^{-1} in the LSR velocity, corresponding to the infall velocity of $\lesssim 0.6$ km s^{-1} without inclination correction, was severely resolved out in our observations. Matter with infalling velocity of $\lesssim 0.6$ km s^{-1} may have structures extending more than 6000 AU, which is the upper limit to the structure detectable in the present observations (see § 2). This is consistent with calculations which show that matter with infall velocity of $\lesssim 0.6$ km s^{-1} will be $\gtrsim 2500$ AU away from a central object of 0.5 $M_\odot$. Thus, the actual size of the infalling disk around L1551-IRS5 may be larger than the derived size from the integrated intensity map. Note that our observations do not tell us whether such an extended infalling envelope still keep a disklike structure or has a more spherical structure as suggested by Butner, Natta, & Evans (1994). In contrast to L1551-IRS5, the infalling disk around HL Tau was not

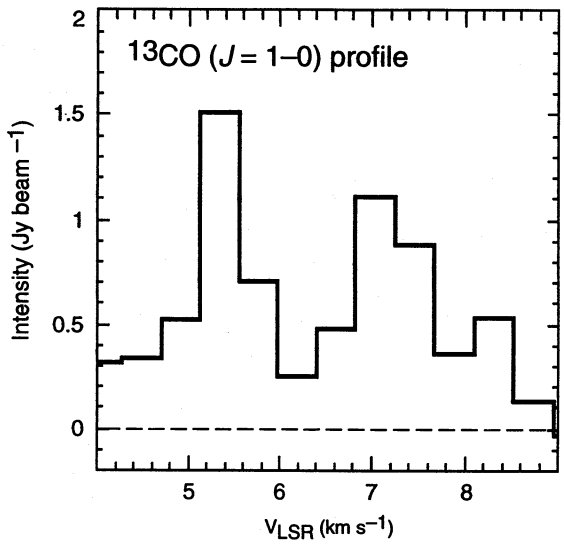

FIG. 5.—^{13}CO ($J = 1$–0) line profile averaged in the 5″ × 5″ area around the position of L1551-IRS5.

remarkably resolved out with the NMA, using the same array configurations, even at velocities close to the systemic velocity (HOM). This suggests that either the infalling disk around L1551-IRS5 is more extended than that around HL Tau, or the disk is more embedded within an extended envelope than the HL Tau disk.

When we compare the present data of ^{13}CO observations of L1551-IRS5 with that of the Nobeyama 45 m telescope, it is found that we detected most of the emission at higher blueshifted ($\sim$4.5–5.8 km s^{-1}) and redshifted ($\sim$7.0–8.2 km s^{-1}) velocities, suggesting that we detected most of the infalling matter with infall velocity $\gtrsim$0.8 km s^{-1} (no inclination correction). This is very reasonable because such infalling matter with higher infalling velocity is located in the vicinity of the central star in the dynamically infalling disk (see § 4.1.). Hence we mainly observed the inner part of the infalling disk around L1551-IRS5 at higher infalling velocity $\gtrsim$0.8 km s^{-1}.

The total mass for the inner part of the disk within $\sim$600 AU in radius can be estimated from the total integrated intensity of the disk using the following formula (Scoville et al. 1986):

$$M_{\rm gas} = 5.37 \times 10^{-5} T_{\rm ex} \exp\left(\frac{5.29}{T_{\rm ex}}\right) \frac{\tau_{^{13}\rm CO}}{1 - \exp\left(-\tau_{^{13}\rm CO}\right)} \times \left(\frac{d}{140\ \rm pc}\right)^2 \left[\frac{10^{-6}}{X(^{13}\rm CO)}\right] \int S_\nu dv\ M_\odot ,$$

where $T_{\rm ex}$ is the excitation temperature, $\tau_{^{13}\rm CO}$ is the optical depth of ^{13}CO, $X(^{13}\rm CO)$ is the fractional abundance of ^{13}CO relative to H_2, and d is the distance to the source. On the assumption of optically thin ^{13}CO, i.e., $\tau_{^{13}\rm CO} \ll 1$, the integrated intensity of 9.12 Jy km s^{-1} for the disk component gives us a disk mass of 1.3×10^{-2} to 2.7×10^{-2} $M_\odot$ with an excitation temperature in the range of 20–50 K and a fractional abundance of 10^{-6}. This mass, however, must be a lower limit to the mass for the inner portion of the disk, because the ^{13}CO emission in the disk may be optically thick. SBKM estimated the optical depth of the C^{18}O emission arising from the disk to be $\sim$0.6 from their interferometric observations, meaning that the optical depth of ^{13}CO is $\sim$3 assuming that the fractional abundance of ^{13}CO to C^{18}O is 5.5. When we use this value for the optical depth of the detected ^{13}CO, the mass is estimated to be 3.9×10^{-2} to 8.1×10^{-2} $M_\odot$ using the same range of the excitation temperature, which is roughly consistent with the mass of the compact C^{18}O disk with a radius of 700 AU observed with OVRO (SBKM).

It should be noted that we may still underestimate the total mass of the disk within 600 AU in radius, because the fractional abundance of ^{13}CO relative to H_2 in the disk might be much smaller than what we assumed. Recent observations with high angular resolution suggested that the abundance of CO molecules, including isotopes, relative to H_2 is 10–100 times smaller in circumstellar disks around T Tauri stars than that in the interstellar medium (Skrutskie et al. 1993; Dutrey, Guilloteau, & Simon 1994; Handa et al. 1995; Saito et al. 1995). Moreover, a theoretical calculation of the molecular abundance in circumstellar disks suggested that CO molecules are depleted at least by one order of magnitude even in 10^5 yr, during which the central source is still embedded like L1551-IRS5 (Aikawa et al. 1996). Hence it may be necessary to treat the estimated gas mass as a lower limit to the actual mass in the following discussion.

Using the estimated mass of the inner portion of the disk, we can estimate the mass infall rate ($\dot{M}$) at the inner portion of the disk by the following formula: $\dot{M} = M_d V_r / R_d$, where R_d is the disk radius, V_r is the radial infall velocity at the radius of R_d, and M_d is the disk mass within the radius of R_d. When we use the minimum detected infall velocity, 0.8/(sin i) km s^{-1} (i; inclination angle of the disk) as the infall velocity at the radius of 600 AU, the mass accretion rate is estimated to be 1.3×10^{-5} to 2.6×10^{-5} $M_\odot$ yr^{-1} assuming the inclination angle of 55°. When we assume an inclination angle of 75°, the estimated accretion rate becomes smaller by a factor of 1.2. We note that the derived mass accretion rate may be underestimated because of the underestimation of the disk mass as was discussed above.

This accretion rate at the radius of 600 AU may be larger than the accretion rate onto the star estimated from the bolometric luminosity of L1551-IRS5 on the assumption of steady accretion ($\dot{M} = \sqrt{L_{\rm bol} R_* / G\tau_*}$, where $L_{\rm bol}$ is the bolometric luminosity, and R_* and τ_* are the radius and the age of the central star; see Kenyon et al. 1990, Ohashi et al. 1991): when we assume that the age of L1551-IRS5 is 10^5 yr, which is a typical age of embedded sources in Taurus (Beichman et al. 1986; Kenyon et al. 1990), the mass accretion rate is estimated to be 6.4×10^{-6} $M_\odot$ yr^{-1} using the bolometric luminosity of 33 $L_\odot$ (Keene & Masson 1990). Although the difference in the estimated accretion rate is only a factor of 2–4, the difference becomes much larger if the accretion rate in the infalling envelope is underestimated from the observation. Thus, the difference in the estimated accretion rate may be significant. If the difference is true, such difference means that mass accretion around L1551-IRS5 is not steady as for the case of HL Tau (HOM; Lin et al. 1994), i.e., the accretion rate is higher at the outer part of the disk than that at the inner part. Actually, L1551-IRS5 is considered to be an FU Orionis object (Stocke et al. 1988; Hartmann, Kenyon, & Hartigan 1993), in which mass accretion is nonsteady (Hartmann & Kenyon 1985). Moreover, recently observed successive ejection events of the molecular outflow of L1551-IRS5 may also suggest outburst phenomenon resulting from nonsteady accretion. Another possibility explaining the discrepancy in the estimated accretion rate is that L1551-IRS5 is younger than other embedded sources in Taurus. If the age of L1551-IRS5 is 10^4 yr, the accretion rate would be estimated to be 2×10^{-5} $M_\odot$ yr^{-1} on the assumption of steady accretion, which is comparable to the accretion rate estimated from the present results. However, the age of the oldest part of the molecular outflow associated with L1551-IRS5 was estimated to be $\sim 10^5$ yr (Bachiller et al. 1994), meaning that the age of L1551-IRS5 may be at least $\sim 10^5$ yr. Hence we may conclude that the accretion around L1551-IRS5 is nonsteady. This result suggests that L1551-IRS5 may be an FU Orionis object in quiescence rather than in an outburst phase. L1551-IRS5 is associated with a more massive compact disk as compared with other embedded sources in Taurus (Ohashi et al. 1991, 1996). The nonsteady accretion around L1551-IRS5 may explain the larger mass of the compact disk (Lin et al. 1994).

5. SUMMARY

We have carried out ^{13}CO(J = 1–0) interferometric observations of L1551-IRS5 using the NMA. A strong and compact condensation coincident with L1551-IRS5, and much weaker extended component elongated from L1551-

IRS5 were detected. Our main results are summarized as follows:

1. The extended component shows U-like features, which roughly delineate the outflow lobes of L1551-IRS5, with blueshifted and redshifted velocities with respect to the systemic velocity. The reflection nebula associated with L1551-IRS5 is surrounded by the blueshifted U-like feature. These properties suggest that the extended component with the U-like features may be part of a dense shell swept up by the outflow, such as the cases observed toward several YSOs.

2. The compact component, marginally resolved with the present angular resolution, shows an elongated structure perpendicular to the optical and radio jets ejected from L1551-IRS5, with size of 1200 × 670 AU. Such an elongated structure is naturally understood as a gaseous disk around L1551-IRS5. The ^{13}CO disk shows a clear velocity gradient along its minor axis. This velocity gradient can be explained in terms of infalling motion in the disk. The position-velocity diagram along the disk minor axis through the central star suggests that the detected motion is consistent with infall in the plane of a disk around a 0.5 $M_\odot$ star.

3. The total mass contained in the ^{13}CO disk was estimated to be 3.9×10^{-2} to 8.1×10^{-2} $M_\odot$, which is underestimated if the CO molecules are depleted in circumstellar disks as suggested by a theoretical calculation as well as actual observations around T Tauri stars. From this mass estimation of the disk, the accretion rate of the disk at 600 AU in radius was estimated to be 1.3×10^{-5} to 2.6×10^{-5} $M_\odot$ yr^{-1}. This mass accretion rate may be larger than that onto the central star estimated from the bolometric luminosity of L1551-IRS5 on the assumption of the steady accretion. This discrepancy suggests that the accretion around L1551-IRS5 may be nonsteady, as was observed around HL Tau.

We acknowledge the staff members of NRO. We are grateful to H. Chen for his assistance in making Figure 1. We thank L. Hartmann, J. Najita, and T. Nakano for fruitful discussion. We also thank an anonymous referee for providing invaluable suggestions which improved this paper. N. O. is supported by a Smithsonian Postdoctoral Fellowship.

REFERENCES

Adams, F. C., Lada, C. J., & Shu, F. H. 1987, ApJ, 312, 788
Aikawa, Y., Miyama, S. M., Nakano, T., & Umebayshi, T. 1996, ApJ, submitted
Bachiller, R., Tafalla, M., & Cernicharo, J. 1994, ApJ, 425, L93
Beichman, C. A., Myers, P. C., Emerson, J. P., Harris, S., Mathieu, R., Benson, P. J., & Jennings, R. E. 1986, ApJ, 307, 337
Butner, H. M., Natta, A., & Evans, N. J., II 1994, ApJ, 420, 326
Cabrit, S., & Bertout, C. 1990, ApJ, 348, 530
Cabrit, S., Guilloteau, S., André, P., Bertout, C., Montmerle, T., & Schuster, K. 1996, A&A, 305, 527
Chikada, Y., et al. 1987, Proc. IEEE, 75(9), 1203
Dutrey, A., Guilloteau, S., & Simon, M. 1994, A&A, 286, 149
Elias, J. 1978, ApJ, 244, 857
Handa, T., et al. 1995, ApJ, 449, 894
Hartmann, L., & Kenyon, S. 1985, ApJ, 299, 462
Hartmann, L., Kenyon, S., & Hartigan, P. 1993, in Protostar and Planets III, ed. E. H. Levy & J. I. Lunine (Tucson: Univ. Arizona Press), 497
Hayashi, M., Ohashi, N., & Miyama, S. M. 1993, ApJ, 418, L71 (HOM)
Hodapp, K.-W. 1994, ApJS, 94, 615
Kaifu, N., et al. 1984, A&A, 134, 7
Keene, J., & Masson, C. R. 1990, ApJ, 355, 635
Kenyon, S. J., Calvet, N., & Hartmann, L. 1993, ApJ, 414, 676
Kenyon, S. J., Hartmann, L. W., Strom, K. M., & Strom, S. E. 1990, AJ, 99, 869
Kitamura, Y., Kawabe, R., & Ishiguro, M. 1992, PASJ, 44, 407
Lay, O. P., Carlstrom, J. E., Hills, R. E., & Phillips, T. G. 1994, ApJ, 434, L75
Lin, D. N. C., Hayashi, M., Bell, K. R., & Ohashi, N. 1994, ApJ, 435, 821
Liseau, R., & Sandell, G. 1986, ApJ, 304, 459
Masson, C. R., & Chernin, L. M. 1992, ApJ, 387, L47
Moriarty-Schieven, G. H., & Snell, R. L. 1988, ApJ, 332, 364
Mundt, R., & Fried, J. 1983, ApJ, 274, L83
Myers, P. C., Bachiller, R., Caselli, P., Fuller, G. A., Mardones, D., Tafalla, M., & Wilner, D. J. 1995, ApJ, 449, L65
Ohashi, N., Hayashi, M., Kawabe, R., & Ishiguro, M. 1996, ApJ, in press
Ohashi, N., Kawabe, R., Hayashi, M., & Ishiguro, M. 1991, AJ, 102, 2054
Rodríguez, L. F., Cantó, J., Torrelles, J. M., & Ho, P. T. P. 1986, ApJ, 301, L25
Saito, M., Kawabe, R., Ishiguro, M., Miyama, S. M., Hayashi, M., Handa, T., Kitamura, Y., & Omodaka, T. 1995, ApJ, 453, 384
Sargent, A. I., Beckwith, S., Keene, J., & Masson, C. 1988, ApJ, 333, 936 (SBKM)
Scoville, N. Z., Sargent, A. I., Sanders, D. B., Claussen, M. J., Masson, C. R., Lo, K. Y., & Phillips, T. G. 1986, ApJ, 303, 416
Skrutskie, M. F., Snell, R. L., Strom, K. M., Strom, S. E., Edwards, S., Fukui, Y., Mizuno, A., Hayashi, M., & Ohashi, N. 1993, ApJ, 409, 422
Snell, R. L., Loren, R. B., & Plambeck, R. L. 1980, ApJ, 239, L17
Snell, R. L., & Schloerb, F. P. 1985, ApJ, 295, 490
Stocke, J. T., Hartigan, P. M., Strom, S. E., Strom, K. M., Anderson, E. R., Hartmann, L. W., & Kenyon, S. J. 1988, ApJS, 68, 229
Sunada, K., Kawabe, R., & Inatani, J. 1993, Int. J. Infrared Millimeter Waves, 14, 1251
Uchida, Y., Kaifu, N., Hayashi, S. S., Hasegawa, T., & Shibata, K. 1987, PASJ, 39, 907
Yang, J., Ohashi, N., & Fukui, Y. 1995, ApJ, 455, 175
Zhou, S. 1992, ApJ, 394, 204
Zhou, S., Evans, N. J., II, Kömpe, C., & Walmsley, C. M. 1993, ApJ, 404, 232